



Planar Slope Failure in Heavily Jointed Rock: Tension Cracks and Nonlinear Strength

Roberto Úcar · Norly Belandria ·
Alfredo Corredor · Luis Arlegui

Received: 5 May 2023 / Accepted: 4 August 2023
© The Author(s) 2023

Abstract This work proposes the calculation of the factor of safety for a strongly jointed rock mass in the case of plane failure with a tensile crack whose exact position or depth is not known but is expected to exist. This calculation is performed by applying the non-linear failure criteria of the Focus Procedure of Úcar and Hoek–Brown's and implementing the necessary formulae in a spreadsheet. The aim is to provide a simple, cost-effective, and easy-to-use procedure that is useful in the early stages of a project or as a starting point for more detailed investigations. Besides slope geometry and strength parameters, the required parameters are the RMR of the rock mass or its m_i , depending on the criterion used. The proposed procedure allows for the estimation of the factor of safety, the position and depth of the tensile crack, and the inclination of the failure plane in the most unfavorable case, with reasonable accuracy, using an iterative process with the conventional tools available in common spreadsheet programs. An example

is provided in which an accuracy of 86–96% for the factor of safety is obtained.

Keywords Factor of safety · Tension crack · Rock failure criteria · Úcar criterion · H–B criterion

1 Introduction

Slopes, and their stability, constitute one of the primary concerns in any civil and mining engineering project (Kirschbaum et al. 2010; Petley 2012; Sasaoka et al. 2015; Heidarzadeh et al. 2019; Jing et al. 2023, Hou et al. 2023). This endeavor becomes considerably complex in rock engineering due to the presence of discontinuities. An immediate consequence of the presence of discontinuities in a rock mass is the formation of discrete rock blocks that vary in size from a few cubic millimeters to several cubic meters. Due to the low-stress state near these free surfaces, the primary factors that influence the dynamic stability of the blocks are their own weight, possible fluid pressures acting on the massif, static loads or overloads, and external dynamic loads, such as those produced by earthquakes. The gross stability of blocks is typically assessed through a factor of safety, denoted as FS, and finding the critical slip surface with the minimum factor of safety is a common goal in geotechnical engineering.

One of the first decisions the rock engineer has to take is how to consider the rock mass (Alzo'ubi

Supplementary Information The online version contains supplementary material available at <https://doi.org/10.1007/s10706-023-02629-9>.

R. Úcar · N. Belandria · A. Corredor
Escuela de Ingeniería Geológica, Universidad de Los
Andes, Mérida, Venezuela

L. Arlegui (✉)
Departamento de Ciencias de la Tierra, Universidad de
Zaragoza, Saragossa, Spain
e-mail: arlegui@unizar.es

2016). On the one hand, by a discreet analysis of kinematics and dynamics taking into account the frictional behavior of present joint sets (weathering, roughness JRC values, ...) and one of the limit equilibrium methods, LEM (De Freitas and Waters 1973; Goodman and Shi 1985; Abramson et al. 2001; Wyllie and Mah 2004; Bar and Barton 2017; Azarafza et al. 2021); on the other, the consideration of the mass as a continuum whole and use finite elements modeling (FEM) and similar robust numerical approaches with constitutive resistance equations, as the Hoek–Brown (H–B) criterion (Jing et al. 2023). Classically, these are two very different approaches to studying rock mass failure and, following Jing and Hudson (2002), we may call them continuum and discrete -discontinuum- analyses. Continuum (FEM, for instance) may make sense, for instance, for Q values (Q-System, Barton et al. 1974) under 0.1 (pseudo continuum for Barton 2021, 2022) or over 100. In intermediate cases, for middling Q values, discontinuum analyses mostly either consider frictional resistance on joint planes, apply distinct element methods (Cundall 1971; Cundall and Hart 1985; Shen and Abbas 2013; Grindheim et al. 2022; Sun et al. 2022; Zhao et al. 2022), or use block theory models (Shi and Goodman 1989).

In heavily jointed rock masses, say with $Q < 0.1$ or $RMR < 30$, the abundance of discontinuities creates uncertainty in the orientation and nature of the critical surface. This, coupled with the presence of a tension crack release surface, leads to a complex stability configuration (Lin and Sheng 2021; Park 2023) that may be better dealt with by considering the resistance of the rock mass rather than deterministically characterizing a discrete joint set.

According to Barton (1971), tension cracks result from small movements within the rock mass, which, although individually small, can accumulate and significantly displace the slope surface. His model determined that the tensile crack generated by tangential movements is a relevant indicator of shear failure initiation within the rock mass. However, Wyllie and Mah (2004) and Wyllie (2017) note that many rock slopes with tensile cracks have not yet failed and have maintained their stability for decades. Nevertheless, the presence of a tensile crack should be considered a potential indicator of instability in any case. Ideally, we would know the position of the tensile crack, but in field surveys, it can be challenging to determine

the exact depth of the crack, as it is often obstructed by rock fragments or sediments. Therefore, it is more conservative to analyze the most critical potential failure block as a function of the distance from the crack to the edge of the slope face. On the other hand, FEM methods, while appropriate for pseudo continuum rock masses, experience difficulties when modeling cases with tension cracks, as the crack must be included as a boundary condition (Park 2023). Moreover, scarce attention has been paid to rock masses with tension cracks, especially when compared to soil slopes, and then applying linear approaches (Zhao et al. 2017), or the H–B criterion (Zhu and Yang 2018; Lee and Pietruszczak 2021).

In such scenarios, it is important to have a failure criterion for the rock mass (Hoek and Brown 1980, 2019; Kulatilake et al. 2006; Úcar 2021), preferably a non-linear one that fits the significant curvature (Barton 2016) of the failure envelope at low normal stresses (as expected in slope stability cases). While Belandria et al. (2021) studied a case where the position of the tension crack was known and applied the Mohr–Coulomb criterion to estimate its shear strength, which was suitable for analyzing well-characterized joint sets, this paper uses a non-linear failure criterion where the position of the critical tension crack is an unknown variable. Additionally, the rock mass is considered to behave as a pseudo continuum rather than a structurally controlled mass where displacement occurs along well-defined joint sets. In these cases, the approach as a continuum model typically involves time-consuming procedures such as finite element, finite difference, and boundary element methods, which require special computational requirements and training to use effectively (Raghuvanshi 2019). Empirical methods based on rock mass classifications are often in use in preliminary stages of stability assessment (Duran and Douglas 2000; Basahel and Mitri 2017).

This paper focuses on the slope stability of a heavily jointed rock mass with tension cracks, where the presence of discontinuities at different attitudes can result in planar failure and the opening of tension cracks upslope. We consider dynamic loads, such as earthquakes, and static overload upslope, as well as pore pressure acting on the tension crack and sliding plane.

The H–B criterion (Hoek and Brown 1980, 2019) is the best-known non-linear criterion for rock

masses. However, in this paper, we explore the application of a novel criterion: Úcar’s Focus procedure, extended to the rock mass case (Úcar 2021).

The procedure presented in this paper provides a useful addition to preliminary surveys. An easy-to-use spreadsheet gives an approximate value of the Factor of Safety, which can then be refined further through more robust and complex modeling approaches.

2 Úcar’s Focus Procedure: Non-linear Strength Criterion

As mentioned earlier, the application of non-linear criteria has long been recognized as a necessity in rock engineering. In this paper, we compare the use of the well-known H–B criterion (Hoek and Brown 1980, 2019) with a novel approach called Úcar’s Focus procedure, which is less well known. To introduce this new criterion (Úcar 2011, 2021), we provide a brief overview of its main points.

In this criterion, the relationship between the major principal stress (σ_1) and the minor principal stress (σ_3) is given by Eq. (1):

$$\bar{\sigma}_1 = k_1(\bar{\sigma}_3 - \xi) + k_2(\bar{\sigma}_3 - \xi)^{1/2} \tag{1}$$

where $\bar{\sigma}_1 = (\sigma_1/\sigma_c)$ and $\bar{\sigma}_3 = (\sigma_3/\sigma_c)$, the constants k_1 and k_2 are material dependent, $\xi = (\sigma_t/\sigma_c)$; σ_c is the uniaxial strength of the rock, and σ_t is the uniaxial tensile strength. This equation is derived from the analysis of the Mohr envelope, which represents the failure envelopes of a set of curves (i.e., Mohr circles) in the $\sigma - \tau$ space obtained by pairs of $\sigma_1 - \sigma_3$ in failure tests, such as uniaxial compression and triaxial tests. The equation obtained by Úcar (2021) describes the envelope in canonical form as a parabola. The criterion can also be expressed in terms of normal and shear stresses. The normal stress σ_n acting in the failure plane can be parametrically expressed as a function of the dip of the tangent to the envelope (β) or the instantaneous friction angle (φ_i), which depends on the stress level, $d\tau_\alpha/d\sigma_n = \tan \beta$. We refer interested readers to Úcar (2011, 2021) for full mathematical development.

On the other hand, considering Eq. (1) and the fact that the family of curves $f(\sigma_n, \tau_\alpha, \sigma_3) = 0$ has

an envelope, Úcar (2021) derived the equation of the envelope, which can be expressed parametrically as:

$$\frac{\sigma_n}{\sigma_c} = \xi + (1 - \sin \beta) \cdot \left\{ k_4 + \left(\frac{k_2}{2(1 + k_1)} \right)^2 \right\} \cdot \left(\frac{4k_1 + (3 - k_1)[(1 - k_1) + (1 + k_1) \sin \beta]}{[(1 - k_1) + (1 + k_1) \sin \beta]^2} \right) \tag{2}$$

And the shear stress, τ_α :

$$\left(\frac{\tau_\alpha}{\sigma_c} \right) = \left(\frac{\sigma_n}{\sigma_c} - \xi \right) \cdot \tan \left(45^\circ + \frac{\beta}{2} \right) - \frac{\left(\frac{k_2}{2} \right)^2 \cdot \tan \left(45^\circ + \frac{\beta}{2} \right)}{\left[\tan^2 \left(45^\circ + \frac{\beta}{2} \right) - k_1 \right]^2} \tag{3}$$

The material constants, k_1 and k_2 , are obtained from the parabola properties as

$$k_1 = k_1(\xi) = \frac{-(1 + |\xi|) + \sqrt{(1 + 7|\xi|)(1 - |\xi|)}}{2|\xi|} \tag{4}$$

and

$$k_2 = k_2(\xi) = \frac{[1 - k_1(-\xi)]}{\sqrt{-\xi}} \tag{5}$$

Their obtention involves the latus rectum concept—the chord through a focus parallel to the conic section directrix (Coxeter 1961)—by applying a coordinates switch (Úcar 2021). Because of this, the author often refers to this criterion as Úcar’s Focus procedure. The constant k_4 , that appears as an integration constant, is obtained from the boundary conditions, for example, by imposing that σ_3 is equal to 0 (uniaxial compression test, so that σ_1 is σ_c).

The criterion is extended to rock masses as

$$\bar{\sigma}_1 = k_1(\bar{\sigma}_3 - \xi_m) + k_2(\bar{\sigma}_3 - \xi_m)^{1/2} \tag{6}$$

where, as before, $\bar{\sigma}_1 = (\sigma_1/\sigma_c)$, $\bar{\sigma}_3 = (\sigma_3/\sigma_c)$, k_1 and k_2 are rock mass dependent constants, and now $\xi_m = (\sigma_{tm}/\sigma_c)$, where σ_c is the uniaxial strength of the intact rock, and σ_{tm} is the tensile strength of the rock mass.

$$k_2 = k_2(\xi_m) = \frac{[\eta_m - k_1(-\xi_m)]}{\sqrt{-\xi_m}} \tag{7}$$

$$k_1 = k_1(\xi_m) = \frac{-(\eta_m + |\xi_m|) + \sqrt{\eta_m^2 + 6 \cdot \eta_m \cdot |\xi_m| - 7\xi_m^2}}{2|\xi_m|} \tag{8}$$

The new constant, η_m , is obtained from the rock mass classification, in this case from the Rock Mass Rating (RMR, Bieniawski 1989), although it could be expressed, as well, as a function of the Geological Strength Index (GSI, Hoek and Brown 2019), Q-system (Barton et al. 1974) or Rock Mass index (RMi, Palmström, 1995):

$$\eta_m = \left(\frac{\sigma_{cm}}{\sigma_c} \right) \approx \exp \left(\frac{RMR - 100}{a_c} \right) \tag{9}$$

The factor a_c varies, according the literature, between $18.75 \leq a_c \leq 24$, as for Ramamurthy (1986), $a_c = 18.75$; for Kalamaras and Bieniawski (1995), $a_c = 24$; and for Sheorey (1997), $a_c = 20$. Finally, the tensile strength of the rock mass is derived from:

$$\xi_m = \left(\frac{\sigma_{im}}{\sigma_c} \right) \approx \xi \cdot \exp \left(\frac{RMR - 100}{14} \right) \tag{10}$$

Therefore, when RMR is 100 (akin to intact rock), it follows that $\xi_m = \xi$. Consequently, when considering the rock mass resistance with Eqs. 1 and 2, parameter ξ is replaced by ξ_m , and similarly, $k_1(\xi)$ and $k_2(\xi)$ become $k_1(\xi_m)$ and $k_2(\xi_m)$, respectively.

In summary, this criterion requires the determination of both the uniaxial compressive and tensile strength of the intact rock, as well as the characterization of the rock mass. It is worth noting that direct tensile strength (DTS) testing is rarely performed due to difficulties in preparing the specimens; many poorly prepared specimens fail invalidly, and adequately lathing specimens to achieve the desired testing shape remains a strong limiting factor (Klanphumeesri 2010; Perras and Diederichs 2014). However, indirect tensile tests, specifically the results of the Brazilian Test (BTS), have been found to provide a reasonably good correlation with DTS, albeit lithology dependent, with $DTS = f \cdot BTS$, where f can be considered approximately 0.9 for metamorphic, 0.8 for igneous, and 0.7 for sedimentary rocks (Perras and Diederichs 2014). The uncertainties associated

with the proposed correlation will likely limit this approach to preliminary design purposes unless triaxial tests are available, and a regression fitting to the data allows for a better determination of ξ .

The relative simplicity (if the direct tensile test is obtained by correlation with the Brazilian test) and ease of obtaining input data make this criterion a very interesting and cost-effective alternative in the preliminary stages of geotechnical surveys.

3 Notation, Geometry, and Dynamics of the Problem

The entire procedure for estimating the factor of safety, as presented here, can be carried out using a spreadsheet (available as supplementary material with this paper). To input the required data into the spreadsheet, we must first define the parameters of the problem.

A common approach to analyzing the rupture surface, both in soils and rock masses, is to divide it into two rupture planes (Gadeus 1970; Kranz 1972; Hoek and Bray 1977; Wyllie and Mah 2004; Priest 2005; Pariseau 2006). An important precursor to rigid block analysis is the determination of kinematic feasibility. A given block is kinematically feasible if it is '... physically capable of being removed from the rock mass without disturbing the adjacent rock' (Priest

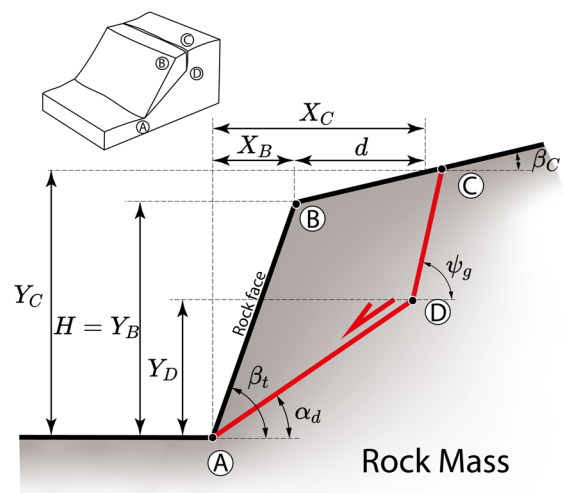


Fig. 1 Slope geometry showing the potential failure plane, and the depth of the tensile crack

1985). Let us, then, consider (Fig. 1) the 2D case of a slope of finite height, where a block is kinematically feasible (Markland 1972; Priest 1993). The geometrical prerequisites for the analysis, following similar models (Hoek and Bray 1977; Priest 1993; Wyllie and Mah 2004), are as follows:

We shall consider the case where a rock face, AB, the potential sliding plane, AD, the top of the slope, BC, and the tension crack, CD, all strike within some 20–25° of each other and intersect to form a kinematically feasible block along the planar discontinuity AD (Fig. 1). The height of the rock face (vertical distance between A and B) is H; it dips β_t , and its upper slope dips β_c . The plane dips $\alpha_d < \beta_t$, so it may daylight at the slope face (Markland 1972), and will intersect at the slope’s toe (maximum volume for the sliding block). Let us assume that a tension crack has developed upslope in the rock mass, possibly along a favorably oriented joint set or by coalescing several pre-existing fractures. The crack reaches an unknown depth z, and its dip angle is denoted by ψ_g . For ease of calculation, we set the slope toe as the coordinate datum (X=0, Y=0). In our case, we seek to determine the most critical block and, consequently, the safety factor.

Regarding forces and stresses (Fig. 2), we will consider a unit width slice perpendicular to the slope face. In tension cracks, opening is the only kinematic consideration in the absence of tangential stress. The tension crack, of vertical depth z, may contain water to a vertical depth z_w . Initially, we will assume $z_w = 0$. Once we determine the critical plane (z and α_d), we can incorporate pore pressure (both in the tension crack and the main plane) and additional loads

(static overload upslope and dynamic seismic loads) into the model to obtain the modified safety factor, F. The maximum water pressure at the base of the tension crack is $u_{max} = \gamma_w \cdot z_w$, where γ_w is the unit weight of water. This water pressure also acts within the sliding plane AD, and possible groundwater pressures configurations are (Wyllie and Mah 2004): uniform pressure on the slide plane for drainage blocked at the toe; triangular pressure on the slide plane for water table below the base of tension crack, or a linear decay to zero at the rock face, also as a triangular distribution, in our case this last configuration, which is probably one of the most commonly in use (see, for instance, Raghuvanshi 2019) has been adopted, as expressed in Fig. 2. The distribution of normal stress acting on the main plane is triangular as well.

In a sense, by adopting this pore pressure distribution it is assumed that only the water in the tension crack and along the slip surface influences slope stability. For Wyllie and Mah (2004) this is tantamount to assuming that the rest of the rock mass is impermeable, an assumption that is certainly not always justified.

The spreadsheet has an input area where the following data are to be specified:

- Geometric parameters: H, β_t , β_c , distance d (horizontal distance from the slope rim to the tension crack daylight in the upslope), ψ_g .
- Force and stress parameters: γ (average bulk weight of the rock mass, in kN/m³), q (overload, in kN/m²), k_h and k_v (seismic accelerations, as fractions of g),
- Resistance parameters: RMR, σ_c (uniaxial strength, in MPa), σ_t (tensile strength, in MPa), a_c and a_t (necessary for the Focus procedure, see Eqs. 7 and 8).

To evaluate the safety factor, F, we need to know the weight of the sliding block, hence its volume. The coordinates of the corresponding vertices, B, C, D, of the block must be determined (vertex A is known: it is the reference point or datum).

Considering the sliding plane AD and the tension crack CD, the coordinates of point D are:

$$Y_D = X_D \cdot \tan \alpha_d \tag{11}$$

where $X_A \leq X \leq X_D$, and

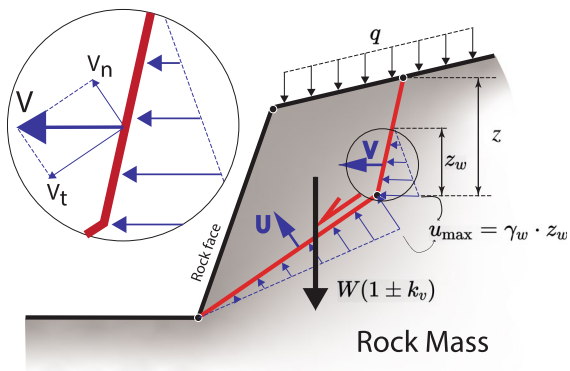


Fig. 2 Force distribution in the slope

$$Y_D = X_D \cdot \tan \psi_g + b \tag{12}$$

where $X_D \leq X \leq X_C$, and b is the intercept. Developing Eqs. (11) and (12), we obtain:

$$X_D = \frac{-\left(\frac{b}{\tan \psi_g}\right)}{1 - \tan \alpha_d \cdot \cot \psi_g} \tag{13}$$

Considering now the point C, of coordinates $X_C = d + H \cot \beta_t$, and $Y_C = d \tan \beta_t + H$, and that additionally, by considering the plane CD, the ordinate at point C is:

$$Y_C = X_C \cdot \tan \psi_g + b \therefore -\frac{b}{\tan \psi_g} = (X_C - Y_C \cdot \cot \psi_g) \tag{14}$$

Replacing X_C and Y_C results in:

$$-\frac{b}{\tan \psi_g} = [d \cdot (1 - \tan \beta_c \cdot \cot \psi_g) + H(\cot \beta_t - \cot \psi_g)] = M \tag{15}$$

Following Priest (1993, 2005), we define M in Eq. (15), as an intermediate geometrical parameter, as M allows us to relate other parameters belonging to the geometry of the slope. On the other hand, the abscissa X_D value depends on X_C through Eqs. 13 and 14) and taking into account that $d = X_C - H \cdot \cot \beta_t$ is also determined in the following expression:

$$X_D = \left(\frac{X_C \cdot (\tan \psi_g - \tan \beta_c) + H \left(\frac{\tan \beta_c}{\tan \beta_t} - 1 \right)}{(\tan \psi_g - \tan \alpha_d)} \right) \tag{16}$$

It is easy to check that $\tan \psi_g \rightarrow \infty \Rightarrow X_D = X_C$, and that M tends towards X_C . Likewise, from Eq. (16), can be obtained:

$$M = X_D(1 - \tan \alpha_d \cdot \cot \psi_g) \tag{17}$$

And from Eqs. (17) and (11) we obtain:

$$Y_D = X_D \cdot \tan \alpha_d = \frac{M}{(\cot \alpha_d - \cot \psi_g)} \tag{18}$$

In Fig. 1 we can observe the meaning of angles β_c and β_t , and also that $\overline{CD} = \frac{(Y_C - Y_D)}{\text{sen} \psi_g}$, and $Z = (Y_C - Y_D) = \overline{CD} \cdot \text{sen} \psi_g$, so

$$Z = (H + d \cdot \tan \beta_c) - \frac{M}{(\cot \alpha_d - \cot \psi_g)} \tag{19}$$

Finally, for clarity in the analytical process, Table 1 summarizes the values of the vertex coordinates of the sliding block. Knowing these values, the area of the polygon ABCDA can be obtained by cross multiplication and knowing that $X_A = 0$ and $X_B = 0$.

$$\text{Area} = \frac{1}{2} [X_C \cdot (Y_B - Y_D) + Y_C \cdot (X_D - X_B)] \tag{20}$$

As we are considering a slice of unit width, the weight of the sliding block derives from:

$$W_T = \frac{\gamma}{2} [X_C(Y_B - Y_D) + Y_C(X_D - X_B)] + q \cdot \left(\overbrace{X_C - X_B}^d \right) \tag{21}$$

The distance d quite often varies between a fifth and a half the height of the slope (Coates 1967). We can easily incorporate other forces into the analysis. For instance, to add seismic dynamic loading we can use the horizontal and vertical acceleration coefficients to evaluate the seismic forces acting in the slope:

$$R = W_T \sqrt{k_h^2 + (1 + k_v^2)} \Rightarrow R = W_T \cdot k \tag{22}$$

where $k = \sqrt{k_h^2 + (1 + k_v^2)}$

Next, X_C is expressed as a function of the depth z of the tensile crack, because later the safety factor will be minimized depending on α_d and z. In Fig. 1 we can observe that $Y_D = Y_C - z$ and $Y_D = X_D \cdot \tan \alpha_d$ (Eq. 11). The equation of the straight line BC comes as

$$Y_C = X_C \tan \beta_t + H \left(1 - \frac{\tan \beta_c}{\tan \beta_t} \right) \tag{23}$$

Equating both ordinates belonging to point D and replacing the value of Y_C given in Eq. (23), and given the value of $X_D = X_C - z \cdot \cot \psi_g$, then the abscissa X_C can be expressed in this way:

$$X_C = \frac{H(1 - \cot \beta_t \cdot \tan \beta_c) - z(1 - \cot \psi_g \cdot \tan \alpha_d)}{(\tan \alpha_d - \tan \beta_c)} \tag{24}$$

Table 1 Coordinates of relevant points and parameters M and d

Point	Coordinate X	Coordinate Y
A	0	0
B	$X_B = \frac{H}{\tan \beta}$	$Y_B = H$
C	$X_C = d + H \cot \beta_i$ $X_C = \frac{H(1 - \cot \beta \cdot \tan \beta_i) - z(1 - \cot \psi \cdot \tan \alpha)}{(\tan \alpha - \tan \beta_i)}$ $X_C = (b_2 - z \cdot b_3)$ $b_2 = \frac{H(1 - \cot \beta \cdot \tan \beta_i)}{(\tan \alpha - \tan \beta_i)}$ $b_3 = \frac{(1 - \cot \psi \cdot \tan \alpha)}{(\tan \alpha - \tan \beta_i)}$	$Y_C = X_C \cdot \tan \beta_i + b_1$ $Y_C = X_C \cdot \tan \beta_i + H \left(1 - \frac{\tan \beta_i}{\tan \beta}\right)$ $Y_C = X_C \cdot \tan \beta_i + b_1$
D	$X_D = \left(\frac{X_C \cdot (\tan \psi_g - \tan \beta_c) + H \left(\frac{\tan \beta_c}{\tan \beta} - 1 \right)}{\tan \psi_g - \tan \alpha_d} \right)$ $X_D = \frac{X_C \cdot (\tan \psi - \tan \beta_i) + H \left(\frac{\tan \beta_i}{\tan \beta} - 1 \right)}{(\tan \psi - \tan \alpha)}$ $= X_C \cdot b_5 - b_6$ $b_5 = \frac{(\tan \psi - \tan \beta_i)}{(\tan \psi - \tan \alpha)}$ $b_6 = \frac{H \left(\frac{\tan \beta_i}{\tan \beta} - 1 \right)}{(\tan \psi - \tan \alpha)}$ $X_D = \frac{Y_D}{\tan \alpha} = \frac{(X_C \cdot \tan \beta_i + b_1) - \lambda \cdot H}{\tan \alpha}$	$Y_D = X_D \cdot \tan \alpha_d = \frac{M}{(\cot \alpha_d - \cot \psi_g)}$ $Y_D = Y_C - z$ $z = \lambda \cdot H$ $Y_D = X_C \cdot \tan \beta_i + b_1 - \lambda \cdot H$
M	$M = d \cdot (1 - \tan \beta_c \cdot \cot \psi_g) + H(\cot \beta_i - \cot \psi_g)$	
d	$d = X_C - X_B = X_C - \frac{H}{\tan \beta}$	

In Fig. 2 it can be observed the maximum pressure due to water occurs at point D, and its value is $u_{\max} = \gamma_w \cdot z_w$. Thus, the resulting hydraulic force U generated by the water pressures that act over the plane of area $AD \cdot 1$ (unit width) equals to

$$U = \frac{1}{2} \gamma_w \cdot z_w \cdot \overline{AD} = \frac{1}{2} \gamma_w \cdot z_w \cdot \frac{Y_D}{\sin \alpha_d} \tag{25}$$

From Eq. (18) we obtain:

$$U = \frac{1}{2} \gamma_w \cdot z_w \cdot \left(\frac{M}{\cos \alpha_d - \sin \alpha_d \cdot \cot \psi_g} \right) \tag{26}$$

At the same time, it has been considered that this interstitial pressure u is acting on the slip plane and decreases to zero at the slope toe. Additionally, the resulting of the interstitial pressure that act over the tensile crack, V, is,

$$V = \frac{1}{2} \gamma_w \cdot z_w^2 \cdot \cos \psi_g \tag{27}$$

On the other hand, from Figs. 2 and 3 the normal and tangential components of V are:

$$V_n = V \cdot \cos (\psi_g - \alpha_d) \tag{28}$$

$$V_t = V \cdot \sin (\psi_g - \alpha_d) \tag{29}$$

and

$$R_t = R \cdot \sin (\alpha_d + \epsilon) = W_T \cdot k \cdot \sin (\alpha_d + \epsilon) \tag{30}$$

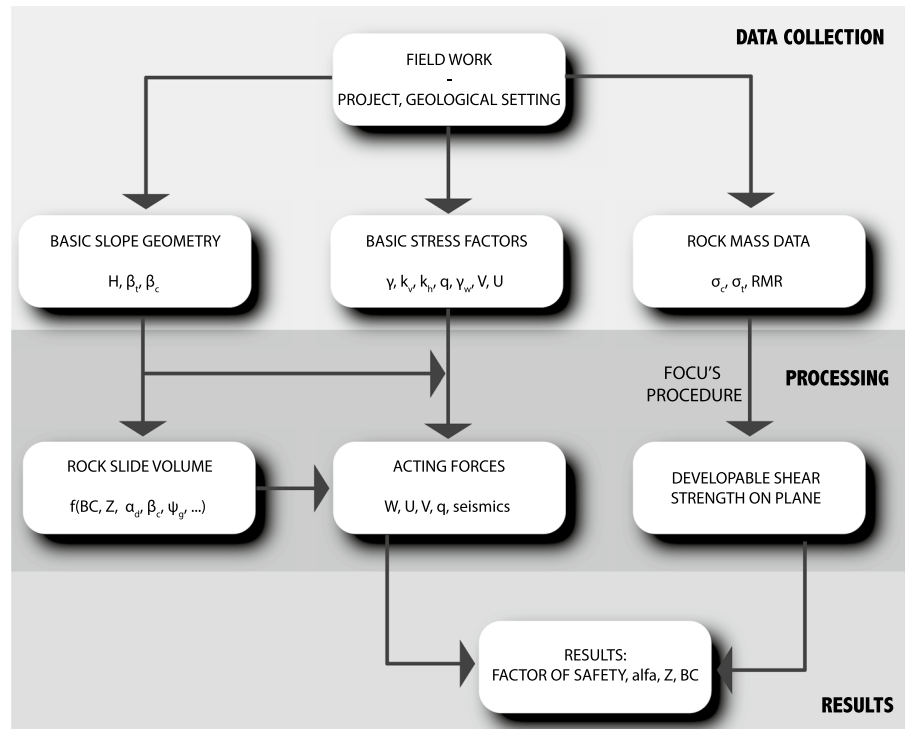
Applying the equilibrium equations results to the normal forces (F_n)

$$\sum F_n = 0 \Rightarrow N + V_n + U - R_n = 0 \tag{31}$$

$$R_n = R \cdot \cos (\alpha_d + \epsilon) = W_T \cdot k \cdot \cos (\alpha_d + \epsilon) \tag{32}$$

where

Fig. 3 Workflow chart



$$N = W_T \cdot k \cdot \cos(\alpha_d + \varepsilon) - U - V \cdot \cos(\psi_g - \alpha_d) \tag{33}$$

On the other hand, with the tangential forces, (F_t)

$$\sum F_t = 0 \Rightarrow T - R_t - V_t = 0 \tag{34}$$

$$T = W_T \cdot k \cdot \sin(\alpha_d + \varepsilon) + V \cdot \sin(\psi_g - \alpha_d) \tag{35}$$

4 Determining the Safety Factor, F

Usually, slope stability is analyzed with limit equilibrium methods and it is expressed as a safety factor. As is well known, it is common practice to determine the safety factor by applying the linear Mohr–Coulomb failure criterion through the equations

$$F = \frac{C \cdot \overline{AD} + (R_n - U - V_n) \tan \phi}{R_t + V_t} \tag{36}$$

$$F = \frac{C \cdot \overline{AD} + (W_T \cdot k \cos(\alpha_d + \varepsilon) - V \cos(\psi_g - \alpha_d) - U) \tan \phi}{(W_T \cdot k \cdot \sin(\alpha_d + \varepsilon) + V \cdot \sin(\psi_g - \alpha_d))} \tag{37}$$

This section describes, in contrast, the procedure for determining the factor of safety by applying two different non-linear failure criteria, those of Úcar and Hoek and Brown (Hoek and Brown 1980, 2019; Úcar 2011, 2021).

4.1 Slope stability assessment with Úcar criterion

We shall consider that the safety factor is constant all over every sliding plane. First, σ'_{np} , the normal effective stress (average value) due to the wedge weight, is determined with Eq. (29). Then, observing Fig. 2 and considering the length of the sliding segment AD, it results in the following equation

$$\sigma'_{np} = \frac{W_T \cdot k \cdot \cos(\alpha_d + \varepsilon) - U - V \cdot \cos(\psi_g - \alpha_d)}{\overline{AD}} = \frac{N}{\overline{AD}} \tag{38}$$

If we modify Eq. (33) to be dimensionless by dividing by σ_c , we can equate Eqs. (2) and (33), obtaining:

$$\left(\frac{1}{\sigma_c}\right) \left[\frac{W_T \cdot k \cdot \cos(\alpha_d + \epsilon) - U - V \cdot \cos(\psi_g - \alpha_d)}{AD} \right] = \xi_m + (1 - \sin \beta) \left\{ k_4 + \left(\frac{k_2}{2(1 + k_1)} \right)^2 \right\} \left[\frac{4k_1 + (3 - k_1)[(1 - k_1) + (1 + k_1) \sin \beta]}{[(1 - k_1) + (1 + k_1) \sin \beta]^2} \right] \tag{39}$$

And likewise, from Eq. (3):

$$\left(\frac{\tau_\alpha}{\sigma_c}\right) = \left(\frac{\sigma_n}{\sigma_c} - \xi_m\right) \cdot \tan\left(45 + \frac{\beta}{2}\right) - \frac{\left(\frac{k_2}{2}\right)^2 \cdot \tan\left(45 + \frac{\beta}{2}\right)^2}{\left[\tan^2\left(45 + \frac{\beta}{2}\right) - k_1\right]^2} \tag{40}$$

At this point, if we know β we can immediately obtain the normal and shear stresses with Eqs. (34) and (35). As the normal stress, σ'_{np} , is actually an average value of the normal stress distribution acting on AD, and must equal to the normal stress expressed by Eq. (34), the obtained values of β will represent in this case average values of the friction angle, ϕ_i , along the sliding surface (Fig. 4).

Finally, the safety factor can be obtained as:

$$F = \frac{\left(\frac{\sigma_n}{\sigma_c} - \xi_m\right) \cdot \tan\left(45^\circ + \frac{\beta}{2}\right) - \frac{\left(\frac{k_2}{2}\right)^2 \cdot \tan\left(45^\circ + \frac{\beta}{2}\right)^2}{\left[\tan^2\left(45^\circ + \frac{\beta}{2}\right) - k_1\right]^2}}{\left(\frac{1}{\sigma_c}\right) \cdot \left(\frac{1}{AD}\right) (W_T \cdot k \cdot \sin(\alpha_d + \epsilon) + V \cdot \sin(\psi_g - \alpha_s))} \tag{41}$$

Now, this expression of the safety factor is a function of AD , that in turn depends on the position of the tension crack (Fig. 1).

$$\overline{AD} = \left(\frac{Y_C - z}{\sin \alpha_d}\right) = \frac{[X_C \cdot \tan \beta_c + b - \lambda \cdot H]}{\sin \alpha_d} \tag{42}$$

It is worth noting the importance of the dimensionless parameter $\lambda = z/H$, which is intended to better understand and analyze the geometry of the wedge as a whole because it indicates which

fraction of the slope height corresponds to the depth of the tensile crack. For example, if $z=0$, then $\lambda = 0$ and, of course, there is no fracture due to traction; and on the contrary, if $z=H$ then $\lambda = 1$, that is to say, the tensile crack corresponds to the slope height. Experience has shown that values of λ are in the interval of 0.20–0.50 (Coates 1967).

Additionally, one can determine the weight of the two potential failure blocks depending on the abscissa X_C , which is $X_C = f(\alpha_d, \lambda)$ considering ψ_g, β_t, β_c , and H constants. This allows a more global and integral vision of the problem by determining the F with respect to the variables λ, α_d , and β . As previously mentioned, β is the inclination of the tangent to the rupture envelope for each value of normal stress. This angle is known as the instantaneous friction angle ($\beta = \phi_i$).

The main advantage is that X_C represents the location of the tensile crack at the crown of the slope, being also the abscissa that serves as a link to determine Y_C of the tensile crack.

The weight in Eq. (22) can be put into function of X_C in this way:

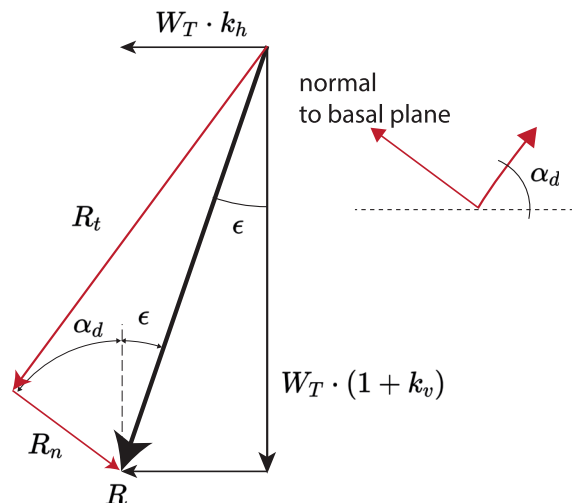


Fig. 4 Force polygon

$$\begin{aligned}
 W_T = & \frac{\gamma}{2}(H \cdot X_C - X_C^2 \tan \beta_c - b_1 \cdot XC + z \cdot X_C \\
 & + \overbrace{[X_C \tan \beta_c + b_1]^2}^{\gamma c^2} \cdot \cot \alpha_d) \\
 & + \frac{\gamma}{2} \cdot (-z \cdot X_C \cdot \tan \beta_c \cdot \cot \alpha_d \\
 & - z \cdot \cot \alpha_d \cdot b_1 - XC \tan \beta_c \cdot H \cdot \cot \beta_t) \\
 & - H \cdot \cot \beta_t \cdot b_1 + q \cdot XC - q \cdot H \cdot \cot \beta_t \quad (43)
 \end{aligned}$$

The value of b_1 is indicated in Table 1. Substituting $z = \lambda \cdot H$, we obtain:

$$\begin{aligned}
 W_T = & \frac{\gamma}{2} \left(H \cdot X_C - X_C^2 \tan \beta_c - b_1 \cdot XC + \lambda \cdot H \cdot X_C + \overbrace{[X_C \tan \beta_c + b_1]^2}^{\gamma c^2} \cdot \cot \alpha_d \right) \\
 & + \frac{\gamma}{2} (-\lambda \cdot H \cdot X_C \cdot \tan \beta_c \cdot \cot \alpha_d - \lambda \cdot H \cdot \cot \alpha_d \cdot b_1 - XC \tan \beta_c \cdot H \cdot \cot \beta_t \\
 & - H \cdot \cot \beta_t \cdot b_1) + q \cdot XC - q \cdot H \cdot \cot \beta_t \quad (44)
 \end{aligned}$$

On the other hand, we already know that $W_T = \eta(\alpha_d, \lambda)$, $AD = \xi(\alpha_d, \lambda)$, $X_C = \zeta(\alpha_d, \lambda)$ and $\sigma_n = \vartheta(\beta)$. It is important to note that, by applying the numerical methods of the Solver add-in program within the spreadsheet, it is possible to determine the minimum safety factor together with the parameters λ , α_d and β quickly. All this without the need to carry out the laborious analytical process of deriving to minimize the safety factor as we will see next.

Another way to calculate the minimum safety factor is by applying the classical mathematical analytical tools, where a new function f , is considered attached to the condition of Eq. (34):

$$\begin{aligned}
 f = & \frac{\left(\frac{\tau_\alpha}{\sigma_c}\right)}{\left(\frac{1}{\sigma_c}\right) \cdot \left(\frac{1}{AD}\right) (W_T \cdot k \cdot \sin(\alpha_d + \epsilon) + V \cdot \sin(\psi_g - \alpha_d))} + \\
 & + \mu \left(\frac{1}{\sigma_c}\right) \left[\frac{W_T \cdot k \cdot \cos(\alpha_d + \epsilon) - U - V \cdot \cos(\psi_g - \alpha_d)}{AD} \right] - \mu \cdot \left(\frac{\sigma_n}{\sigma_c}\right) \quad (45)
 \end{aligned}$$

In Eq. (39), the terms (τ_α/σ_c) and (σ_n/σ_c) correspond to Eqs. (34) and (35) and were obtained by Úcar (2021) and μ is the Lagrange's multiplier. Thus, to calculate the minimum safety factor, the following derivatives are required:

$$\frac{\partial f}{\partial \alpha_d} = f_{\alpha_d} = 0$$

$$\frac{\partial f}{\partial \varphi_i} = f_{\varphi_i} = 0$$

$$\frac{\partial f}{\partial \mu} = f_\mu = 0$$

Undoubtedly, calculating these derivatives involves a painstaking and laborious process, in addition to having to subsequently solve the system of non-linear equations to determine the parameters λ , α_d and β . Fortunately, all this is solvable in a few seconds by applying the useful numerical tools and their algorithms through the Solver add-in by constraining the problem with the appropriate conditions.

4.2 Slope stability Assessment with Hoek and Brown's Failure Criterion

Taking into account the H-B criterion, Kumar (1998) determined the rupture envelope and the normal tension for the general case of $a \geq 1/2$ by means of a simple analytical procedure, without the need to solve any differential equation; as previously found by Úcar (1986), using the original equation that relates the main stresses σ_1 and σ_3 of such a criterion, by means of the well-known quadratic equation represented by the following equation, that is to say $a = 1/2$.

$$\frac{\sigma_1}{\sigma_c} = \frac{\sigma_3}{\sigma_c} + \left[m \cdot \frac{\sigma_3}{\sigma_c} + s \right]^{1/2} \quad (46)$$

Considering the values of τ_α and σ_n obtained by Kumar (1998) and whose expressions are given below, the calculation procedure is otherwise exactly the same as described in Sect. 4.1:

Kumar's Eqs. (17) and (20):

$$\frac{\tau}{\sigma_c} = \left(\frac{m \cdot a}{2}\right)^{\left(\frac{a}{1-a}\right)} \left(\frac{1 - \sin \phi_i}{\sin \phi_i}\right)^{\left(\frac{a}{1-a}\right)} \left(\frac{\cos \phi_i}{2}\right) \quad (47)$$

$$\begin{aligned}
 \frac{\sigma}{\sigma_c} = & \frac{1}{m} \cdot \left(\frac{m \cdot a}{2}\right)^{\left(\frac{1}{1-a}\right)} \cdot \left(\frac{1 - \sin \phi_i}{\sin \phi_i}\right)^{\left(\frac{1}{1-a}\right)} \\
 & \cdot \left(1 + \frac{\sin \phi_i}{a}\right) - \frac{s}{m} \quad (48)
 \end{aligned}$$

Therefore, the expression of the safety factor is:

$$F = \frac{\left\{ \left(\frac{ma}{2} \right)^{\left(\frac{a}{1-a} \right)} \left(\frac{1-\sin \phi_i}{\sin \phi_i} \right)^{\left(\frac{a}{1-a} \right)} \left(\frac{\cos \phi_i}{2} \right) \right\}}{\left(\frac{1}{\sigma_c} \right) \cdot \left(\frac{1}{AD} \right) (W_T \cdot k \cdot \sin(\alpha_d + \varepsilon) + V \cdot \sin(\psi_g - \alpha_d))} \quad (49)$$

5 Influence of Water Pressure on Stability

The presence of groundwater in a rock slope has several detrimental effects on stability (Wyllie 2017): Water pressure reduces the shear resistance of potential failure surfaces. When present in tension cracks, it increases the forces that favor sliding. Water accelerates weathering and decreases the shear strength of intact rock. Freezing of groundwater can cause wedging in water-filled fissures. Also, ice can block drainage paths. Excavation costs can be increased when working below the water table. In any case, the most important effect of groundwater in a rock mass is the reduction in stability resulting from water pressures within the discontinuities.

There are two possible approaches to introducing water pressure distributions into stability calculations: either applying a flow pattern deduced from the distribution of discontinuities, and their hydraulic conductivities, or obtaining data from direct measurements of water levels in wells, or of water pressure by means of piezometers installed in boreholes.

Obviously, given the multiplicity of possible geometric scenarios of fluid pressure distribution, in the absence of other data, we will apply the model most frequently used in these cases, albeit some caution is warranted; in this regard, (Wyllie 2017) recommends analyzing the sensitivity of our slope-problem to a variety of realistic fluid pressure distributions, paying particular attention to rapid recharge phenomena and the transient pressures that may generate. The considered case, with water present in the tension crack hydraulically connected to the water generating pressure on the sliding surface, probably is a worst-case scenario or close enough to it.

In this procedure, we proceed at first as if there is no water in the rock mass and, once z , α_d and F are determined in dry conditions, it is possible to incorporate different values of z_w (water height within the tension crack) to explore the detrimental effect of water in the F .

6 Step by Step Procedure with the Spreadsheet and SOLVER

As previously mentioned, the full procedure can be implemented via a dedicated spreadsheet available as supplementary material with this paper, it includes a detailed step-by-step procedure. The spreadsheet has an input area where relevant data on the studied slope can be included in the model. The presented equations are employed to determine the value of the factor of safety, and its value is then minimized by varying the geometric parameters to obtain the worst-case scenario. Solver is an add-in program for spreadsheets that can find an optimal (maximum or minimum) value for a formula in one cell—called the Objective cell, which in our case contains the Factor of Safety—subject to constraints, or limits, on the values of other formula cells on a worksheet. Simply put, it serves to determine the maximum or minimum value of one cell by changing other cells.

6.1 Instructions for Using the Spreadsheet

This spreadsheet comprises two sheets that should be used sequentially. The parameters entered in the first sheet are automatically transferred to the second sheet. The reason for structuring it into two sheets is so that SOLVER does not need to be configured each time.

We start on the [parameters] sheet.

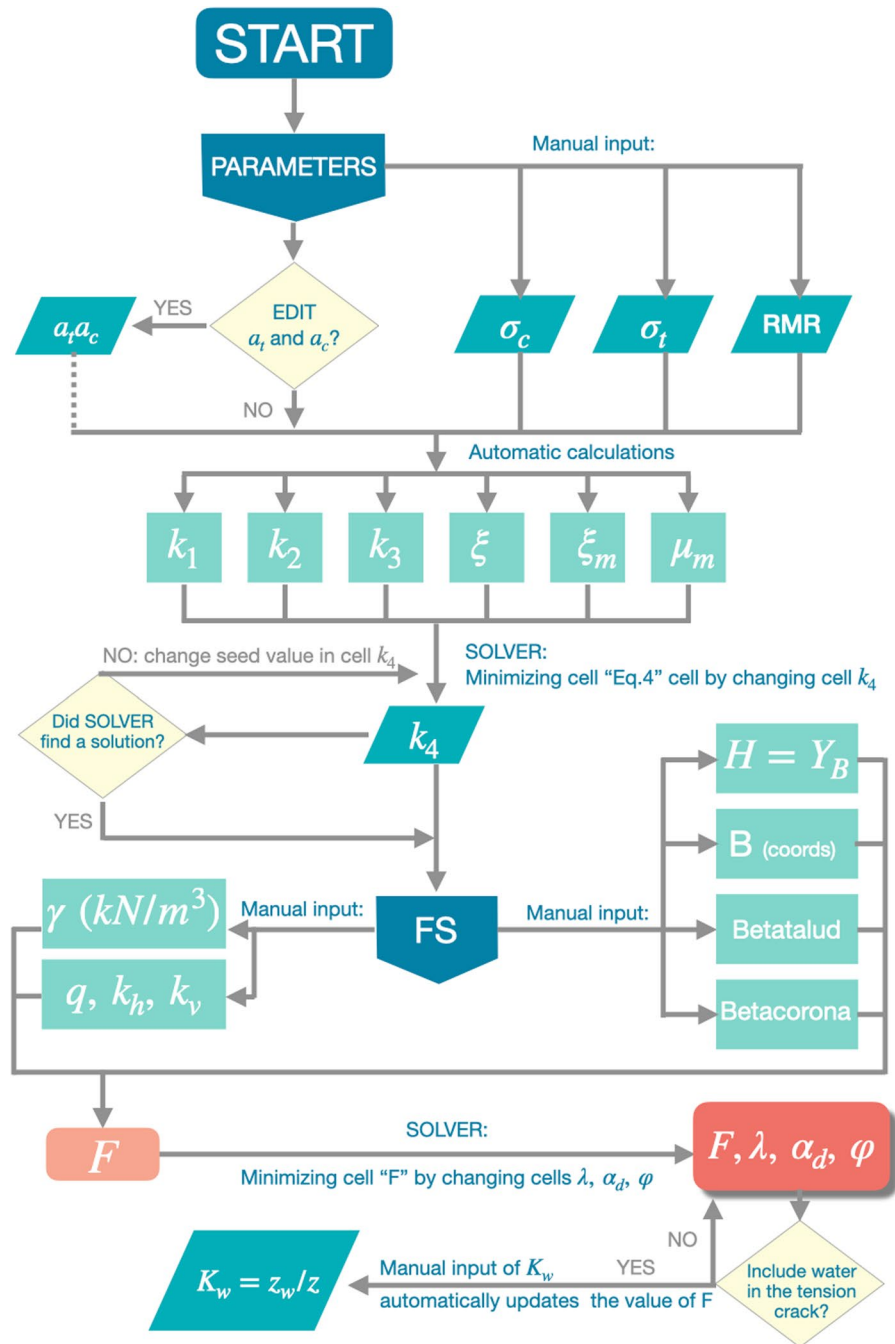
1. Enter the starting parameters. Under the header "1 PARAMETERS" there are cells for entering the uniaxial compressive strength of intact rock (σ_c), tensile strength (σ_t), and the RMR value of the rock mass. Additionally, we can vary the values assigned to the constants a_t and a_c . By default, they appear as $a_t = 14$ and $a_c = 20$, as seen in previous paragraphs.

When these parameters are entered, the spreadsheet automatically computes the values of ξ , ξ_m , μ_m , and the constants k_1 , k_2 , and k_3 .

2. Obtain k_4 . We must obtain k_4 in an iterative process using SOLVER, with the target being cell "Eq. k4" making it equal to zero by modifying the cell "solver adj" (under the cell labeled K4).

Now we move to the [FS] sheet.

Fig. 5 Flowchart for safety factor calculation in the spreadsheet



We check that the sheet has successfully captured the values entered in step 1, as well as the calculations performed: s , k_1 , k_2 , k_3 , and k_4 .

3. Input of basic slope geometry (see Fig. 1 for guidelines, and notice the location of the spatial datum at the toe of the slope for coordinates determination). Enter the height of the slope

(in cell Y_B , under cell $H = Y_B$), coordinates of point B, slope inclination in degrees (under the cell labeled "BETAtalud"), and inclination of the crest of the slope in degrees (under the cell labeled "BETAcrona").

4. Enter the average bulk weight of the rock present in the slope (in kN/m^3).

Table 2 Geometry and mechanical and elastic properties

Property	Value	Unit
Slope Height	H=52	m
Slope dip	76°	
Slope crown dip	$\beta_{crown} = 10^\circ$	
Unit weigh	$\gamma = 25$	kN/m ³
Overburden	q=300	kPa
Horizontal and vertical seismic coefficients	$k_h = 0.2$ and $k_v = 0.1$	
Angle of internal friction	$\phi = 26^\circ$	
Poisson's coefficient	$\nu = 0, 25$	
Elasticity modulus	$E = 25, 00E6$	kPa
Uniaxial compressive strength	$\sigma_c = 48$	MPa
Rock Mass Rating	$RMR = 55$	
Material constant	$m_i = 12$	
Disturbance factor	$D = 0$	

Table 3 Summary of results

	Úcar's	Hoek and Brown's	SLIDE	PLAXIS 2D
F	2.392	2.067	2.292	2.133
d(m)	17.28	16.28	19.29	20.00
z(m)	18.18	17.14	9.75	16.00
α	50.64°	52.23°	52.00°	48.68°

- Enter, if necessary, the overload on the crest of the slope, and the horizontal and vertical seismic acceleration coefficients, k_h and k_v .
- Apply SOLVER to obtain the value of the safety factor, F. The target cell is F, minimizing its value by changing the cells λ (relative depth of the tensile crack), α_d (dip of the failure plane), and ϕ (instantaneous friction angle), subject to the conditions that X_C is greater than or equal to X_B , d is less than or equal to d_s and greater than or equal to d_l , δ is equal to zero, and λ is between zero and one. In this step, once we obtain the minimized value of F, the values in cells λ and α_d reflect now the relative depth of the tensile crack, and the dip of the failure plane, determining the geometry of the sliding block in the critical condition.
- Once the basic value of F has been obtained, we can add the effect of the presence of water

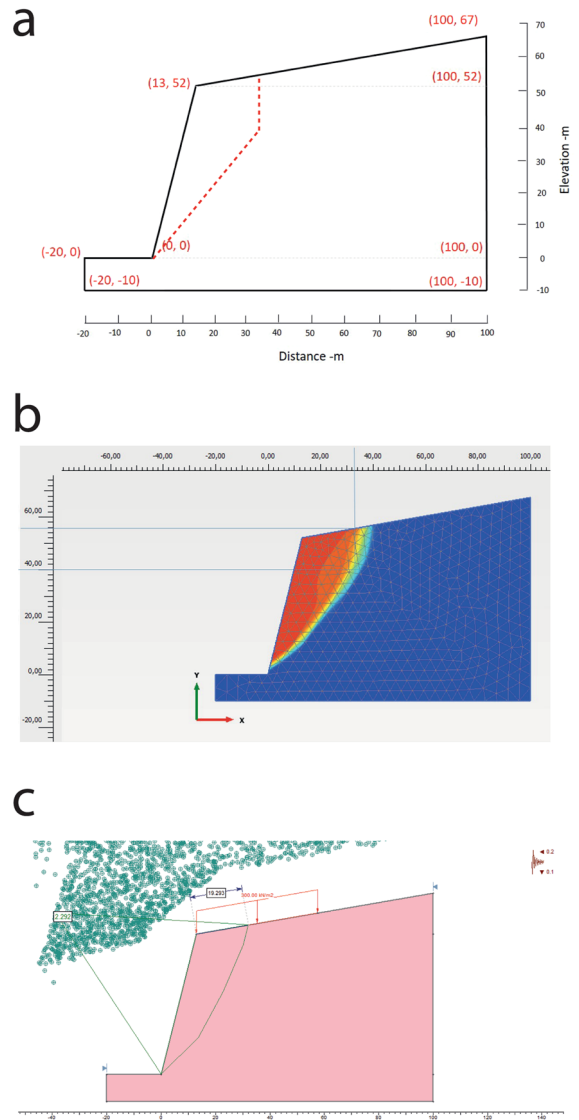


Fig. 6 Comparison of results of the different methods for the proposed example. **a** Geometry of the case. Red dashed line, results of the method proposed in this work. **b** Crack surface generated by Finite Element Method (Plaxis 2D). **c** Results obtained through the Limit Equilibrium Method (SLIDE). The FS, the distance of the tensile crack at the slope crest and the depth of the tensile crack are shown

on the slope by introducing the factor K_w , the ratio between z_w and z . The safety factor will be updated accordingly.

A flow chart illustrating this procedure is in Fig. 5.

7 Worked Example: Comparing Results Between Using H–B Criterion, Úcar Criterion, Limit Equilibrium Method (Slide), and Finite Element Method (Plaxis 2D) with an Idealized Slope

The geometric characteristics and mechanical and elastic properties of the slope under study are presented in Table 2. From the simulations using the finite element and limit equilibrium method and analytically with the H–B criterion for the analyzed slope, and comparing their results with the proposed analytical method of the Úcar criterion, it is observed (see Table 3 and Fig. 6):

For the case with seismic loading and linear overload, the FS with the Úcar criterion yielded a value of 2.392. The correlation percentages with respect to the other 3 methods are between 86.42 and 95.82%.

The distance of the formation of the tensile crack at the head of the slope by the Úcar criterion is 17.28 m and the correlation percentages are between 94.22 and 84.26%. For the tensile crack depth 18.18 m of the Úcar criterion, the percentage correlations would be 53.64 and 94.28%. It should be noted that the value of 53.64% corresponds to that obtained by the limit equilibrium method and its correspondence is low, however for the other two methods the correspondence is very good, being above 88.01%. Finally, when comparing the dip of the rupture surface, which in the case of the Úcar rupture criterion is obtained $\beta = 50.64^\circ$, the percentage value of correspondence with the other methods are between 96.13 and 97.32%.

The results show that there is a good correlation and a high correspondence of the proposed method with the Úcar breakage criterion with the other methods because most of the results are above 90% correlation.

8 Conclusions

We present a method for calculating or estimating the factor of safety in a highly jointed rock mass, considering plane failure with an unknown depth of a tensile crack. The Úcar's Focus Procedure and Hoek and Brown's failure criteria are applied by implementing the necessary formulas in a spreadsheet. The required parameters include the slope geometry, strength

parameters, and either the RMR of the massif or its m_i , depending on the chosen criterion. An iterative process with conventional tools is used to obtain an estimate of the safety factor. The resulting value is reasonably close, with a similarity degree of around 86–96% in the solved example, to that obtained with more sophisticated numerical calculation tools. Thus, the proposed procedure is a useful and cost-effective contribution in the early stages of a project or as a starting point for more detailed investigations.

Acknowledgements This work is a contribution of the Geotransfer Research Group (E32_23R), funded by Gobierno de Aragón, and Grupo de Investigación en Geología Aplicada (GIGA), University of Los Andes, Venezuela.

Author Contributions All authors contributed to the study conception and design. The first draft of the manuscript was written by RÚ and LA, and all authors commented on previous versions of the manuscript. NB performed the numerical analysis with PLAXIS and SLIDE. All authors read and approved the final manuscript.

Funding Open Access funding provided thanks to the CRUE-CSIC agreement with Springer Nature.

Data Availability Enquiries about data availability should be directed to the authors.

Declarations

Conflict of interest The authors have no relevant financial or non-financial interests to disclose.

Open Access This article is licensed under a Creative Commons Attribution 4.0 International License, which permits use, sharing, adaptation, distribution and reproduction in any medium or format, as long as you give appropriate credit to the original author(s) and the source, provide a link to the Creative Commons licence, and indicate if changes were made. The images or other third party material in this article are included in the article's Creative Commons licence, unless indicated otherwise in a credit line to the material. If material is not included in the article's Creative Commons licence and your intended use is not permitted by statutory regulation or exceeds the permitted use, you will need to obtain permission directly from the copyright holder. To view a copy of this licence, visit <http://creativecommons.org/licenses/by/4.0/>.

References

- Abramson LW, Lee TS, Sharma S, Boyce GM (2001) Slope stability and stabilization methods, 2nd edn. John Wiley and Sons, INC., New York, London
- Alzoubi AK (2016) Rock slopes processes and recommended methods for analysis. Int J Geomate 11(25):2520–2527

- Azarafza M, Akgün H, Ghazifard A et al (2021) Discontinuous rock slope stability analysis by limit equilibrium approaches—a review. *Int J Digit Earth* 14(12):1918–1941. <https://doi.org/10.1080/17538947.2021.1988163>
- Bar N, Barton N (2017) The Q-slope method for rock slope engineering. *Rock Mech Rock Eng* 50:3307–3322. <https://doi.org/10.1007/s00603-017-1305-0>
- Barton N (1971) A model study of the behaviour of steep excavated rock slopes. PhD thesis, Univ. of London
- Barton N (2016) Non-linear shear strength for rock, rock joints, rockfill and interfaces. *Innov Infrastruct Solut*. <https://doi.org/10.1007/s41062-016-0011-1>
- Barton N (2021) Continuum or discontinuum GSI or JRC ?. In: Geotechnical challenges in mining, tunnelling and underground structures
- Barton N (2022) Keynote lecture: Continuum or discontinuum—that is the question. In: IX Latin American rock mechanics symposium
- Barton N, Lien R, Lunde J (1974) Engineering classification of rock masses for the design of tunnel support. *Rock Mech* 6(4):189–236. <https://doi.org/10.1007/BF01239496>
- Basahel H, Mitri H (2017) Application of rock mass classification systems to rock slope stability assessment: a case study. *J Rock Mech Geotech Eng* 9(6):993–1009. <https://doi.org/10.1016/j.jrmge.2017.07.007>
- Belandria N, Úcar R, Corredor A, Ferri H (2021) Safety factor on rock slopes with tensile cracks using numerical and limit equilibrium models. *Geotech Geol Eng* 39(3):2287–2300. <https://doi.org/10.1007/s10706-020-01624-8>
- Bieniawski Z (1989) Engineering rock mass classifications: a complete manual for engineers and geologists in mining, civil and petroleum engineering. John Wiley and Sons, INC., New York, London
- Coates D (1967) Rock mechanics principles. Mines branch monograph 874, Canada Department of Energy, Mines and Resources
- Coxeter H (1961) Introduction to geometry, 2nd edn. John Wiley and Sons, INC., New York, London
- Cundall PA (1971) A computer model for simulating progressive large scale movements in blocky rock systems. In: Proc. sym. ISRM, Nancy, France [Paper II-8]
- Cundall PA, Hart R (1985) Development of generalized 2-D and 3-D distinct element programs for modelling jointed rock. Tech. rep., U.S. Army Corps of Engineers, Vicksburg
- Duran A, Douglas K (2000) Experience with empirical rock slope design. In: ISRM international symposium, OnePetro
- de Freitas MH, Watters RJ (1973) Some field examples of toppling failure. *Géotechnique* 23(4):495–513. <https://doi.org/10.1680/geot.1973.23.4.495>
- Gadeus G (1970) Lower and upper bound for stability of earth retaining structures. In: Proceedings of the 5th European conference SMFEL, Madrid
- Goodman RE, Shi G (1985) Block theory and its application to rock engineering. Prentice Hall
- Grindheim B, Aasbø KS, Høyen AH et al (2022) Small block model tests for the behaviour of a blocky rock mass under a concentrated rock anchor load. *Geotech Geol Eng* 40(12):5813–5830
- Heidarzadeh S, Saeidi A, Rouleau A (2019) Evaluation of the effect of geometrical parameters on slope probability of failure in the open stoping method using numerical modeling. *Int J Min Sci Technol* 29(3):399–408. <https://doi.org/10.1016/j.ijmst.2018.05.011>
- Hoek E, Bray J (1977) Rock slope engineering, 2nd edn. Institution of Mining and Metallurgy
- Hoek E, Brown E (1980) Empirical strength criterion for rock masses. *J Geotech Eng Div ASCE*. <https://doi.org/10.1061/AJGEB6.0001029>
- Hoek E, Brown E (2019) The Hoek-Brown failure criterion and GSI—2018 edition. *J Rock Mech Geotech Eng*. <https://doi.org/10.1016/j.jrmge.2018.08.001>
- Hou D, Zheng X, Zhou Y et al (2023) Analysis and application of surrounding rock mechanical parameters of jointed rock tunnel based on digital photography. *Geotech Geol Eng* 41(2):721–739. <https://doi.org/10.1007/s10706-022-02298-0>
- Jing HW, Yang XX, Zhang ML (2023) Strength and failure behaviors of a jointed rock mass anchored by steel bolts: a numerical modeling study. *Geotech Geol Eng* 41(1):225–241. <https://doi.org/10.1007/s10706-022-02275-7>
- Jing L, Hudson J (2002) Numerical methods in rock mechanics. *Int J Rock Mech Min Sci* 39(4):409–427
- Kalamaras G, Bieniawski Z (1995) A rock mass strength concept for coal seams incorporating the effect of time. In: 8th ISRM Congress, OnePetro
- Kirschbaum DB, Adler R, Hong Y et al (2010) A global landslide catalog for hazard applications: method, results, and limitations. *Nat Hazards* 52(3):561–575. <https://doi.org/10.1007/s11069-009-9401-4>
- Klanphumesri S (2010) Direct tension testing of rock specimens. Ph.D. thesis, School of Geotechnology Institute of Engineering Suranaree University of Technology
- Kranz E (1972) Bureau of securitas, ground anchors, French Code of Practice
- Kulatilake PHSW, Park J, Malama B (2006) A new rock mass failure criterion for biaxial loading conditions. *Geotech Geol Eng* 24(4):871–888. <https://doi.org/10.1007/s10706-005-7465-9>
- Kumar P (1998) Shear failure envelope of Hoek-Brown criterion for rockmass. *Tunn Undergr Space Technol* 13(4):453–458
- Lee YK, Pietruszczak S (2021) Limit equilibrium analysis incorporating the generalized Hoek-Brown criterion. *Rock Mech Rock Eng* 54(9):4407–4418. <https://doi.org/10.1007/s00603-021-02518-8>
- Lin H, Sheng B (2021) Failure characteristics of complicated random jointed rock mass under compressive-shear loading. *Geotech Geol Eng* 39(5):3417–3435. <https://doi.org/10.1007/s10706-021-01701-6>
- Markland JT (1972) A useful technique for estimating the stability of rock slopes when the rigid wedge slide type of failure is expected. Interdepartmental Rock Mechanics Project, Imperial College of Science and Technology
- Palmström A (1995) Rmi—a system for characterizing rock mass strength for use in rock engineering. *J Rock Mech Tunn Technol* 1(2):69–108

- Pariseau W (2006) Design analysis in rock mechanics, 1st edn. CRC Press
- Park D (2023) Stability evaluation of rock slopes with cracks using limit analysis. *Rock Mech Rock Eng* 56(7):4779–4797. <https://doi.org/10.1007/s00603-023-03281-8>
- Perras MA, Diederichs MS (2014) A review of the tensile strength of rock: concepts and testing. *Geotech Geol Eng* 32(2):525–546
- Petley D (2012) Global patterns of loss of life from landslides. *Geology* 40(10):927–930. <https://doi.org/10.1130/G33217.1>
- Priest S (1985) Hemispherical projection methods in rock mechanics. Allen & Unwin, London
- Priest SD (1993) Discontinuity analysis for rock engineering. Springer Science and Business Media
- Priest S (2005) Determination of shear strength and three-dimensional yield strength for the Hoek-Brown criterion. *Rock Mech Rock Eng* 38(4):299–327
- Raghuvanshi TK (2019) Plane failure in rock slopes—a review on stability analysis techniques. *J King Saud Univ Sci* 31(1):101–109. <https://doi.org/10.1016/j.jksus.2017.06.004>
- Ramamurthy T (1986) Stability of rock mass. *Indian Geotech J* 16(1):1–74
- Sasaoka T, Takamoto H, Shimada H et al (2015) Surface subsidence due to under-ground mining operation under weak geological condition in Indonesia. *J Rock Mech Geotech Eng* 7(3):337–344. <https://doi.org/10.1016/j.jrmge.2015.01.007>
- Shen H, Abbas SM (2013) Rock slope reliability analysis based on distinct element method and random set theory. *Int J Rock Mech Min Sci* 61:15–22. <https://doi.org/10.1016/j.ijrmms.2013.02.003>
- Sheorey P (1997) Empirical rock failure criteria. AA Balkema
- Shi Gh, Goodman RE (1989) Generalization of two-dimensional discontinuous deformation analysis for forward modelling. *Int J Numer Anal Meth Geomech* 13(4):359–380
- Sun L, Grasselli G, Liu Q et al (2022) The role of discontinuities in rock slope stability: insights from a combined finite-discrete element simulation. *Comput Geotech* 147:104788. <https://doi.org/10.1016/j.compgeo.2022.104788>
- Úcar R (1986) Determination of shear failure envelope in rock masses. *J Geotech Eng* 112(3):303–315. [https://doi.org/10.1061/\(ASCE\)0733-9410\(1986\)112:3\(303\)](https://doi.org/10.1061/(ASCE)0733-9410(1986)112:3(303))
- Úcar R (2011) Una metodología reciente para determinar la resistencia al corte en macizos rocosos. In: Proceedings of PanAm CGS geotechnical conference, Toronto, Canada, p 2694
- Úcar R (2021) Determination of a new failure criterion for rock mass and concrete. *Geotech Geol Eng* 39(5):3795–3813. <https://doi.org/10.1007/s10706-021-01728-9>
- Wyllie DC (2017) Rock slope engineering: civil applications. CRC Press
- Wyllie DC, Mah C (2004) Rock slope engineering. CRC Press
- Zhu JQ, Yang XL (2018) Probabilistic stability analysis of rock slopes with cracks. *Geomech Eng* 16(6):655–667
- Zhao L, Cheng X, Li L et al (2017) Seismic displacement along a log-spiral failure surface with crack using rock Hoek-Brown failure criterion. *Soil Dyn Earthq Eng* 99:74–85. <https://doi.org/10.1016/j.soildyn.2017.04.019>
- Zhao T, Crosta GB, Liu Y (2022) Analysis of slope fracturing under transient earth-quake loading by random discrete element method. *Int J Rock Mech Min Sci* 157:105171

Publisher's Note Springer Nature remains neutral with regard to jurisdictional claims in published maps and institutional affiliations.